Date: December 28, 2010

Agreement Number: G09AC00093

Title: High-Resolution Urban True Orthoimagery

Final Report

Organization: Old Dominion University
5238 Hampton Road
Norfolk, VA 23529

Principal Investigator: Guoqing Zhou
Kaufman Hall, Rm. 214
Old Dominion University
Norfolk, VA 23529
Tel: (757) 683-3619
Fax: (757) 683-5655
E-mail: gzhou@odu.edu

Executive Summary

The project, entitled "High-Resolution Urban True Orthoimagery Standard", was conducted from July 2009 through November 2010. First, two tele-conferences were held for initial deployment of the proposed project after reviewed by two peer-reviewers specified by FGDC. Six original aerial images captured at downtown Denver, Colorado were used for evaluation of traditional orthoimage generation method. The results demonstrated the problems of such as ghost images, occlusion and building lean, shadow of the buildings, inaccuracy of DSM, incomplete refilling to occlusion, different geometric accuracy of adjacent orthoimages, etc. For this reason, the project presents a method which first established mathematical model of constrain condition, such as perpendicularity, parallel, and then merged these conditions into the orthorectification model. The same data set was used to test the new method. The results demonstrated that the proposed method can improve the accuracy of 2-7 feet for those buildings of over 100 m high. A draft of document pertain to urban gray and color−infrared high-resolution orthoimagery (e.g., 6-inch or one-foot), including process, method, theory, accuracy and quality control, has been produced. In the meanwhile, the survey and evaluation form for high-resolution urban orthoimagery standard was conducted by in-person investigations, mails and telephones. The results indicated that the existent software exposed some problems for urban high-resolution orthoimage generation, but the suggested Standards increase the procedures, cost and time. The outreach was conducted at the PI's course with an enrollment of 20 students. Lecture note, presentation, laboratory class data, and problems-solving exercises have been developed.

Table of Contents

SYMBOLS, ABBREVIATED TERMS, AND NOTATIONS

DTM – Digital Terrain Model

DBM – Digital Building Model

DSM – Digital Surface Model

DOI – Digital Orthoimagery

NTOI – Near True Orthoimagery

SOI – Slavery Orthoimagery

TOI – True Orthoimagery

TIN – Triangulated Irregular Network

List of Figures

List of Tables

Project Narrative

Digital orthophotos (also *orthoimages*) are a critical component of the National Spatial Data Infrastructure (NSDI) (Federal Geographic Data Committee, 1997). The digital orthophotos (1) serve as a geospatial foundation to which an organization may add detail and attach attribute information; (2) provide a base on which an organization can accurately register and compile other themes of data; and (3) orient and link the results of an application to the landscape (Federal Geographic Data Committee, 1995).

Theoretically, the digital orthophoto should be a spatially accurate image with ground features represented in their correct, upright, and true planimetric positions with all distortions removal including lens distortion, terrain relief displacement, and atmospheric distortion. Therefore, the orthophoto contains both the image characteristics of a photograph and the geometric qualities of a map.

1. Challenges of High-Resolution Urban True Orthoimagery

1.1 Test of Urban High-Resolution Urban True Orthoimagery

An experimental field is located in downtown Denver, Colorado, where the highest building is 125m, and many others are around 100m. Six original aerial images are acquired from two flight strips using RC30 aerial camera at a focal length of 153.022 mm on April 1, 2000. The flying height was approximately 1650 m above the mean ground elevation of the imaged area. The aerial photos were originally recorded on film and later scanned into digital format at a pixel resolution of 25μm. Part of the scanned aerial images is shown as Fig. 1a. Fig. 1b is the 2D representation of the digital surface model (DSM).

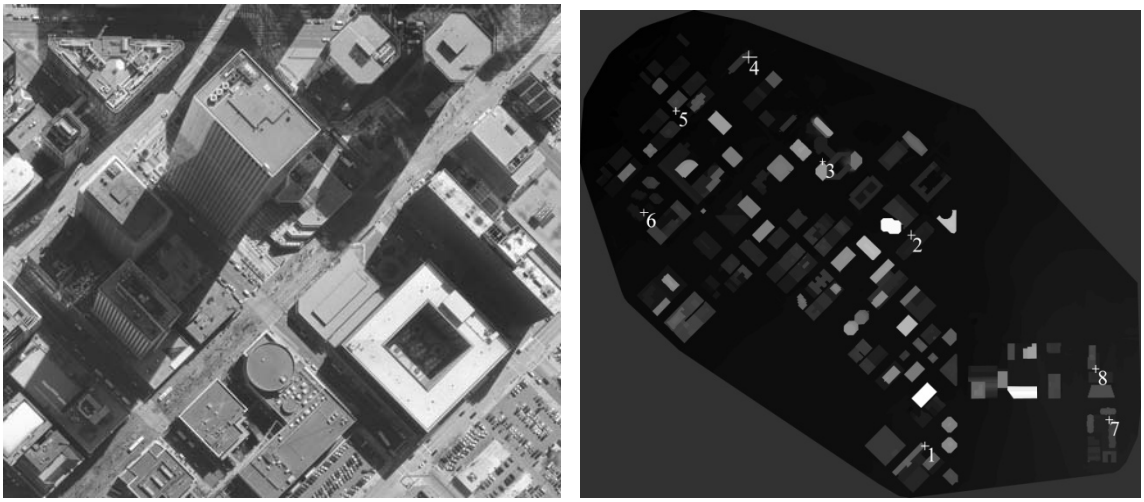

Figure 1 (a) Part of original aerial images of DV1119 and (b) digital surface model in downtown, Denver CO, in which the brightness in the DSM represents surface height

With these parameters and ERDAS/IMAGINE software, we produced the orthoimage of DV1119, as shown in Figure 2. From Figure 2, the following observations have been made.

1.1.1 Ghost images

As observed from Figure 2, although the high buildings can be correctly orthorectified into their upright positions, the roofs of buildings are superimposed onto the bottom of the buildings and the roofs of buildings appear twice. This phenomenon is called "ghost image" (Zhou et al. 2005; 2008). The reason causing ghost images is due to the fact that the higher buildings occlude other objects, and the existing differential rectification model cannot compensate for the occlusion, leading to the result that the occluding objects remain, and the occluded objects cannot be detected and filled. During the orthorectification of images, the brightness of any pixel in the resulting orthoimage is assigned from the corresponding pixel's brightness in the original image using the collinearity equation. Both the resulting orthoimage and the original image share the identical DSM. When we orthorectify the relief displacement caused by buildings, the roofs of buildings are orthorectified in their upright positions; when we orthorectify the relief displacement caused by occluded objects, the occluding objects are again employed to fill the occluded objects. This kind of processing process leads to the occluding pixels to be doubly

employed: the first is for the roof and the second for the occluded objects. Thus, double roofs of the identical building are seen in the resulting orthoimage.

1.1.2 Occlusion and Building Lean

Again as observed in Figure 2, perspective displacements and occlusions still remain in the resulting orthoimage. The orthorectification of the image is partly geometrically inaccurate and/or incomplete; the image features are distorted from their true locations. This distortion appears in the form of leaning buildings. As illustrated in Figure 2, a tall building leans over a street and occludes features like street, manholes, fire hydrants, and utility poles. The existing differential rectification model is not able to identify occlusions and compensates for the occlusions. Thus, the problem is how we can identify and compensate for the occlusion in urban areas considering the occlusion is an inherent property of perspective projection.

Figure 2 Part of the orthorectified image of downtown Denver generated by the differential model

1.1.3 Shadow of the buildings

Shadow of the buildings is another important concern in urban areas. Figure 2 also demonstrates that the shadow cannot be removed using the differential rectification model. As observed in Figure 2, the shadow of the tall building deteriorates the quality of orthoimage, as a result, it is hard to identify the shadowed objects like buildings, bridges, fire hydrants, etc. In order to produce high quality orthoimages, shadows must be removed.

1.1.4 Inaccuracy of DSM

The differential rectification method is based on digital surface model (DSM), which is used to represent and model the buildings. As observed in Figure 3, we found that (1) small objects on top of the building were not completely orthorectified due to the lack of model; (2) the wall of the buildings is incompletely orthorectified due to inaccuracy of the DSM; (3) the boundary of buildings is inaccurately orthorectified due to the inaccuracy of the DSM. Thus, accuracy of the DSM will greatly affect the quality of orthorectification. In fact, it has been demonstrated that the traditional DSM to represent the urban surface objects cannot obtain high-quality orthoimage since the DSM cannot accurately model the details of buildings, i.e., edges of buildings.

Figure 3 Incomplete orthorectification of buildings due to inaccuracy DSM and the lack of detailed representation

1.1.5 Incomplete Refilling to Occlusion

It is unavoidable to have occlusion in urban large-scale images. One of the tasks is therefore to identify the occluded areas from one orthoimage, called *master orthoimage*, and refill them from neighboring orthoimages, called "*slave orthoimage*" (Zhou et al. 2005; 2008). We orthorectified the DV1119 and DV1120 images and manually identified the occluded areas in the DV1119 orthoimage (master) and refilled the occluded areas from the DV1120 orthoimage (slave). As observed in Figure 4, it is not possible to find sufficient slave orthoimages to completely refill the occluded areas in the master orthoimage. This is especially true for those areas containing tall buildings located in the margin of images, where the occlusions are large due to the inherent

property of perspective projection. The cause for incomplete refilling to the occluded areas is because of the low endlap of two adjacent images. Therefore how we design flight mission, such as endlap, sidelap, flying height, choose a camera with different focal length and IFOV, and the direction of flight need to be investigated.

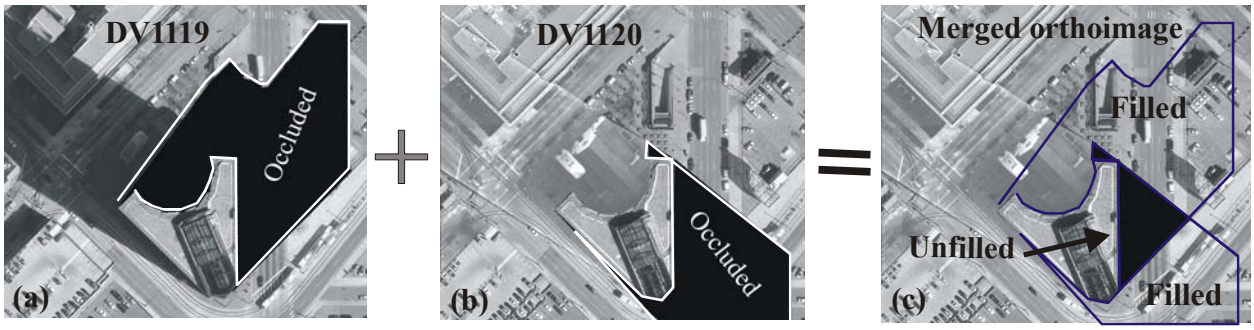

Figure 4 Building occlusion in a master image (a) and slave image (b), resulting in incomplete refilling in resulting image (c).

1.1.6 Different Geometric Accuracy of Two Adjacent Orthoimages

Occlusion refilling requires that the rectified master and all slave orthoimages have the consistent geometric accuracy. We checked the geometric accuracy of the orthoimage DV1119 and DV1120, both of which were generated using the same method (differential rectification model), the same DSM, the same GCPs, and the same iterative number. It is observed that the building in the DV1120 orthoimage was incompletely and inaccurately orthorectified to its planimetric position since the wall information is still visible in Figure 5b (building leaning over), whereas the wall information in the DV 1119 orthoimage is missing, which means the building is completely orthorectified in its upright position (see Figure 5a). This phenomenon is probably caused by the incomplete correction of lens distortion because magnitude of the lens distortion is the function of object locations in an image plane. A building, when imaged in different positions in the adjacent images, has different magnitude of lens distortions.

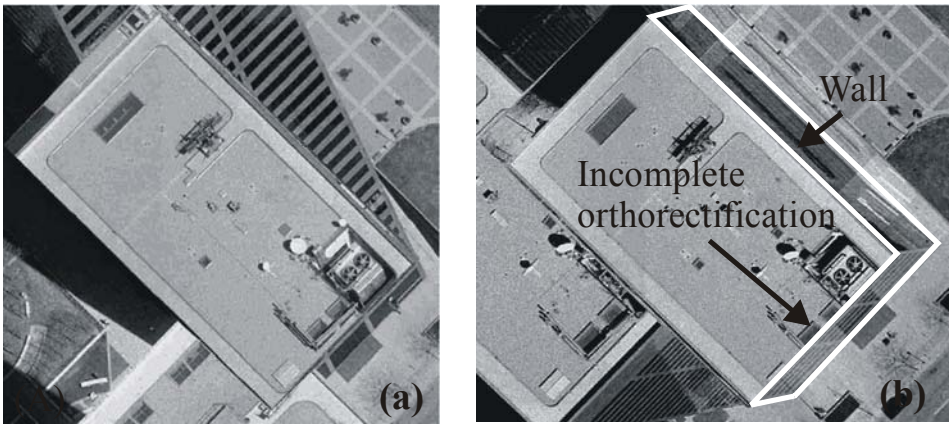

Figure 5 Comparison of orthorectification accuracy for the same building in two neighboring images using the same DSM, (a) DV1119 orthoimage, and (b) DV1120 orthoimage.

It can be imagined that if we employ the different geometric accuracy of slave orthoimages to refill the occluded area of master orthoimage, the final orthoimage contains the geometric errors along with the seam lines, which probably are not seamless. Figure 6 demonstrated the existence of this type of errors. As measured in Figure 6, the same feature in the two orthoimages has an obvious shift of about 7 to 20 pixels.

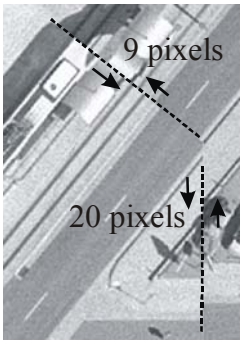

Figure 6 Shift of the same features in the neighbor images when mosaicked.

1.1.7 Radiometric Difference of Two Adjacent Orthoimages

Brightness difference between scene and scene is significant. This phenomenon in urban area is more apparent due to occlusion and shadow. The generation of mosaicking two orthoimages usually requires the occlusion refilling using the slave orthoimages, for which the radiometric difference of the different orthoimages should be kept minimum. Figure 7 illustrates an obvious

radiometric contrast along the seam line, in which the gray difference between the master orthoimage and the slave orthoimage is large.

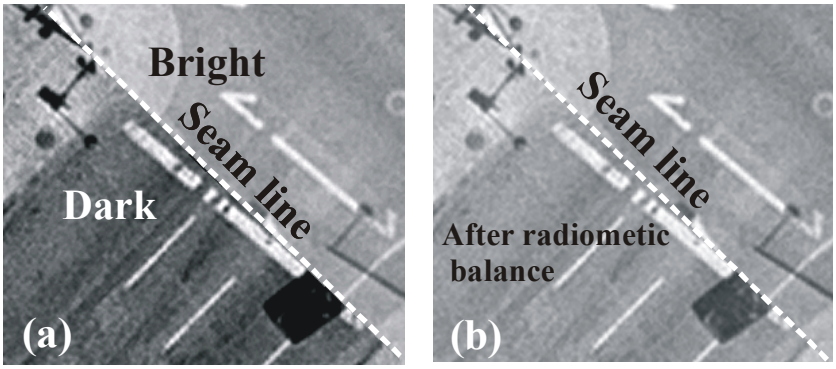

Figure 7 The radiometric contrast along the seam line between "master" and "slave" orthoimages

1.2 Summary of Challenges

The investigation for orthorectification of high-resolution aerial images in urban areas using traditional differential rectification model has discovered the following problems:

(1) *The problems occurring in single orthoimage.* The automatic identification and compensation of the building occlusion are a key step. Unsuccessful processing to this problem causes the phenomena of "ghost images" in the resulting orthoimage. Another main problem is shadow detection and removal. Unsuccessful processing to this problem causes the low quality orthoimage, i.e., visible seamlines, obvious radiometric difference along seamlines. Therefore identification and compensation of occlusion and shadow need to be conducted for urban orthoimages generation. Additionally, inaccuracy of the DSM representation causes rough edges of building and inaccurate geometric position of edges of buildings. The lack of the detailed representation to the small objects results in incomplete orthorectification for urban images. Therefore, an accurate model to represent urban buildings needs to be developed.

(2) *The problems occurring between two orthoimages.* Difference in geometric and radiometric accuracy between two orthoimages can lead to the incomplete refilling of the occluded areas when mosaicked. To minimize the difference in geometric accuracy between two orthoimages, all of distortions should be corrected, and to minimize the

difference in radiometric difference,, the "best" patches in slave orthoimages and optimum seamline should be chosen.

Overall, the existence of these problems indicates that the conventional orthorectification method is not able to orthorectify the objects into their correct and upright positions for a high-resolution urban aerial image. Significant efforts are still needed to improve the methodology for generation of orthoimages.

2. Developed Approaches

2.1Traditional Orthorectification Model

The mathematical model of traditional orthorectification is a called *photogrammetry differential model*, with which, for any given ground point such as G, it is expressed by

$$x_g - x_0 = -f\frac{a_1(X_G - X_S) + b_1(Y_G - Y_S) + c_1(Z_G - Z_S)}{a_3(X_G - X_S) + b_3(Y_G - Y_S) + c_3(Z_G - Z_S)} \qquad (1a)$$

$$y_g - y_0 = -f\frac{a_2(X_G - X_S) + b_2(Y_G - Y_S) + c_2(Z_G - Z_S)}{a_3(X_G - X_S) + b_3(Y_G - Y_S) + c_3(Z_G - Z_S)} \qquad (1b)$$

where f, x_0, y_0 are the camera's interior orientation parameters (IOPs), X_S, Y_S, Z_S are the position of exposure station, $a_1,...,c_3$ are the elements of rotation matrix, which is a functions of three rotation angles ω, φ, κ; x_g, y_g are image coordinate of the ground point G, X_G, Y_G, Z_G are the coordinates of the ground point G in ground coordinate system.

Eq. 1 can further be expressed by a linear equation after it is linearized using Taylor's series, i.e.,

$$\boldsymbol{V} = \boldsymbol{AT} - \boldsymbol{L} \qquad (2)$$

Where $\boldsymbol{T} = (\varphi\ \omega\ \kappa\ X_S\ Y_S\ Z_S)^T$, $\boldsymbol{V} = (v_{gx_1}\ v_{gy_1}\ v_{gx_2}\ v_{gy_2})^T$, $\boldsymbol{L} = (l_{gx_1}\ l_{gy_1}\ l_{gx_2}\ l_{gy_2})^T$, A is coefficient. With a number of GCPs, the nominal IOPs provided by the vendor can be calibrated, and the EOPs in Eq. 2 can be solved using least-squares estimation. Once the IOPs and EOPs were determined, any ground point can be orthorectified onto a pre-defined orthogonal plane.

In order to increase the accuracy of orthoimage, one used to increase the number of ground control points (GCPs) and/or select well-distributed GCPs. This method has its limitation because the location and distribution of GCPs impact the accuracy of orthorectification, while the most of the current GCPs are distributed on the ground, which means the top of high building has no sufficient control information. Thus, this paper plans using relative constrain conditions, such as perpendicular and collinear conditions, to improve the accuracy. The mathematical models are below.

2.2 Perpendicular Control Condition

Suppose that AB and BC are two edges of a flat house roof, and their corresponding edges in image plane are ab and bc. Suppose that the coordinates of A, B and C are (X_A, Y_A, Z_A), (X_B, Y_B, Z_B) and (X_C, Y_C, Z_C) in the object coordinate system. For a flat-roof cube house, the heights (i.e., Z coordinates) of A, B, and C are the same, and the line segments AB and BC are perpendicular to each other.

If AB is not perpendicular to BC at an intersection angle θ, i.e., B deviates from its correct position at B′, we draw a line from C to O, and make the line, CO is perpendicular to AB′ (see Figure 8), l is the distance of B and O, and can be expressed by

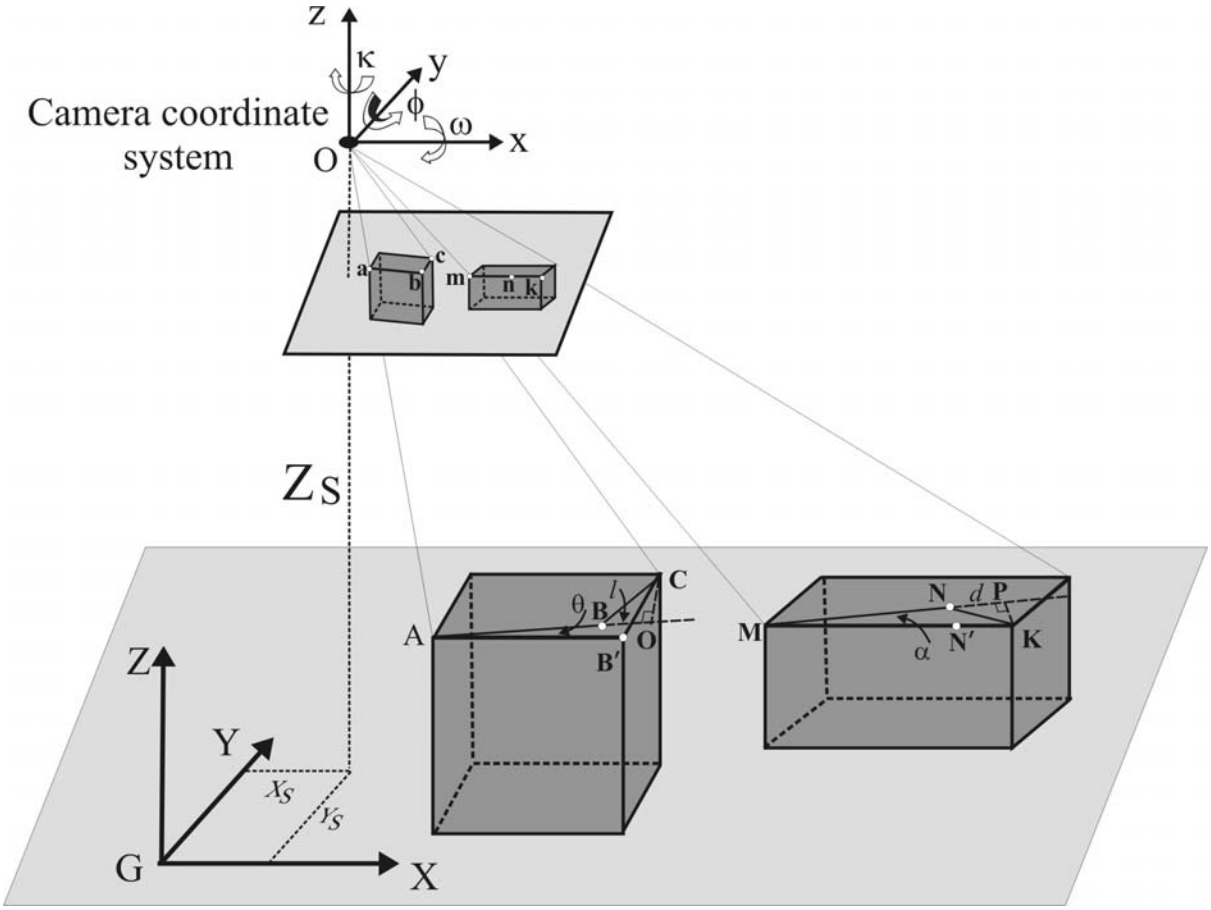

Figure 8 The geometry for perpendicular constraint and collinear constraint condition

$$l = (X_C - X_B)\cos\theta + (Y_C - Y_B)\sin\theta = (X_C - X_B)\frac{(X_B - X_A)}{s_{AB}} + (Y_C - Y_B)\frac{(Y_B - Y_A)}{s_{AB}} \tag{3}$$

where s_{AB} is the distance of the segment AB. Theoretically the distance *l* should be zero. Thus, the differential form for Eq. 3 is:

$$\begin{aligned} l_0 + \Delta l = {} & [(X_C - X_B)\frac{(X_B - X_A)}{s_{AB}} + (Y_C - Y_B)\frac{(Y_B - Y_A)}{s_{AB}}] + \\ & \frac{1}{s_{AB}}[(X_B - X_A)\Delta X_C + (Y_B - Y_A)\Delta Y_C + (X_B - X_C)\Delta X_A + (Y_B - Y_C)\Delta Y_A + \\ & + (X_C - 2X_B + X_A)\Delta X_B + (Y_C - 2Y_B + Y_A)\Delta Y_B] = 0 \end{aligned} \tag{4}$$

Rewrite Eq. 4 by matrix form:

$$\begin{bmatrix} X_B - X_C \\ Y_B - Y_C \\ X_C - 2X_B + X_A \\ Y_C - 2Y_B + Y_A \\ X_B - X_A \\ Y_B - Y_A \end{bmatrix}^T \begin{bmatrix} \Delta X_A \\ \Delta Y_A \\ \Delta X_B \\ \Delta Y_B \\ \Delta X_C \\ \Delta Y_C \end{bmatrix} + \left[(X_C - X_B)(X_B - X_A) + (Y_C - Y_B)(Y_B - Y_A) \right] = 0 \qquad (5)$$

Eq. 5 is in fact a perpendicular constrain condition, which describes line AB perpendicular to BC on the X-Y plane. Similarly, if the point B and C on the plane X-Z, or Y-Z, the perpendicular relative constrain conditions can be expressed by, respectively,

$$\begin{bmatrix} X_B - X_C \\ Z_B - Z_C \\ X_C - 2X_B + X_A \\ Z_C - 2Z_B + Z_A \\ X_B - X_A \\ Z_B - Z_A \end{bmatrix}^T \begin{bmatrix} \Delta X_A \\ \Delta Z_A \\ \Delta X_B \\ \Delta Z_B \\ \Delta X_C \\ \Delta Z_C \end{bmatrix} + \left[(X_C - X_B)(X_B - X_A) + (Z_C - Z_B)(Z_B - Z_A) \right] = 0 \qquad (6)$$

$$\begin{bmatrix} Y_B - Y_C \\ Z_B - Z_C \\ Y_C - 2Y_B + Y_A \\ Z_C - 2Z_B + Z_A \\ Y_B - Y_A \\ Z_B - Z_A \end{bmatrix}^T \begin{bmatrix} \Delta Y_A \\ \Delta Z_A \\ \Delta Y_B \\ \Delta Z_B \\ \Delta Y_C \\ \Delta Z_C \end{bmatrix} + \left[(Z_C - Z_B)(Z_B - Z_A) + (Y_C - Y_B)(Y_B - Y_A) \right] = 0 \qquad (7)$$

The vector form for Eq. 5 can be rewritten by (Eqs. 6 and 7 are similar)

$$\boldsymbol{C_1 \hat{X}_1 + W_1 = 0} \qquad (8)$$

where $\boldsymbol{C_1} = \begin{bmatrix} X_B - X_C \\ Y_B - Y_C \\ X_C - 2X_B + X_A \\ Y_C - 2Y_B + Y_A \\ X_B - X_A \\ Y_B - Y_A \end{bmatrix}^T$, $\boldsymbol{\hat{X}_1} = \begin{bmatrix} \Delta X_A \\ \Delta Y_A \\ \Delta X_B \\ \Delta Y_B \\ \Delta X_C \\ \Delta Y_C \end{bmatrix}$, $\boldsymbol{W_1} =$

$(X_C - X_B)(X_B - X_A) + (Y_C - Y_B)(Y_B - Y_A)$

2.3 Collinear Constrain Condition

Also, as depicted in Figure 8, suppose that the segments MN and NK are not collinear, at an intersection angle of α, we have

$$d = (Y_K - Y_N)\cos\alpha + (X_K - X_N)\sin\alpha = (Y_K - Y_N)\frac{(X_N - X_M)}{s_{MN}} + (X_K - X_N)\frac{(Y_N - Y_M)}{s_{MN}} \qquad (9)$$

where *d* is the distance of between K and P. Similarly, its linearized equation and matrix form are, respectively

$$\begin{aligned} d_0 + \Delta d = {} & [(Y_K - Y_N)\frac{(X_N - X_M)}{s_{MN}} + (X_K - X_N)\frac{(Y_N - Y_M)}{s_{MN}}] \\ & + \frac{1}{s_{MN}}[(Y_N - Y_M)\Delta X_K + (X_N - X_M)\Delta Y_K + (Y_N - Y_K)\Delta X_M + (X_N - X_K)\Delta Y_M \\ & + (Y_K - 2Y_N + Y_M)\Delta X_N + (X_M - 2X_N + X_K)\Delta Y_N] = 0 \end{aligned} \qquad (10)$$

$$\begin{bmatrix} Y_N - Y_K \\ X_K - X_N \\ Y_K - 2Y_N + Y_M \\ X_M - 2X_N + X_K \\ Y_M - Y_N \\ X_N - X_M \end{bmatrix}^T \begin{bmatrix} \Delta X_M \\ \Delta Y_M \\ \Delta X_N \\ \Delta Y_N \\ \Delta X_K \\ \Delta Y_K \end{bmatrix} + \left[(Y_K - Y_N)(X_N - X_M) + (X_K - X_N)(Y_N - Y_M)\right] = 0 \qquad (11)$$

Eq. 11 is in fact a collinear constrain condition, which describes line MN collinear with NK on the X-Y plane. Similarly, if the point M, N, and K on the plane X-Z, or Y-Z, the corresponding collinear constrain conditions are, respectively,

$$\begin{bmatrix} Z_N - Z_K \\ X_K - X_N \\ Z_K - 2Z_N + Z_M \\ X_M - 2X_N + X_K \\ Z_M - Z_N \\ X_N - X_M \end{bmatrix}^T \begin{bmatrix} \Delta X_M \\ \Delta Z_M \\ \Delta X_N \\ \Delta Z_N \\ \Delta X_K \\ \Delta Z_K \end{bmatrix} + \left[(Z_K - Z_N)(X_N - X_M) + (X_K - X_N)(Z_N - Z_M)\right] = 0 \qquad (12)$$

$$\begin{bmatrix} Z_N - Z_K \\ Y_K - Y_N \\ Z_K - 2Z_N + Z_M \\ Y_M - 2Y_N + Y_K \\ Z_M - Z_N \\ X_N - X_M \end{bmatrix}^T \begin{bmatrix} \Delta Y_M \\ \Delta Z_M \\ \Delta Y_N \\ \Delta Z_N \\ \Delta Y_K \\ \Delta Z_K \end{bmatrix} + \left[(Z_K - Z_N)(Y_N - Y_M) + (Y_K - Y_N)(Z_N - Z_M) \right] = 0 \qquad (13)$$

The vector form for Eq. 11 can be written by (Eqs. 12 and 13 are similar)

$$\boldsymbol{C_2}\hat{\boldsymbol{X}}_{\boldsymbol{2}} + \boldsymbol{W_2} = \boldsymbol{0} \qquad (14)$$

where $\boldsymbol{C}_2 = \begin{bmatrix} Z_N - Z_K \\ Y_K - Y_N \\ Z_K - 2Z_N + Z_M \\ Y_M - 2Y_N + Y_K \\ Z_M - Z_N \\ X_N - X_M \end{bmatrix}^T$, $\hat{\boldsymbol{X}}_{\boldsymbol{2}} = \begin{bmatrix} \Delta Y_M \\ \Delta Z_M \\ \Delta Y_N \\ \Delta Z_N \\ \Delta Y_K \\ \Delta Z_K \end{bmatrix}$, $\boldsymbol{W}_2 = (Z_K - Z_N)(Y_N - Y_M) + (Y_K - Y_N)(Z_N - Z_M)$

From Figure 8, if points, A, B and C and their corresponding imaged points, a, b, and c are simultaneously GCPs, this means that one perpendicular or collinear constraint condition will add six additional unknown parameters (i.e., $\Delta X_A, \Delta Y_A, \Delta Z_A, \Delta X_B, \Delta Y_B, \Delta Z_B$ for perpendicular constrain). Thus, Eq.2 can be extended into:

$$\mathbf{V} = \mathbf{AT} + \mathbf{B}\hat{\mathbf{X}} - \mathbf{L} \qquad (15)$$

where, $\boldsymbol{T} = \left(\varphi\ \omega\ \kappa\ X_S\ Y_S\ Z_S \right)^T$,

$\hat{\boldsymbol{X}} = \left(\Delta X_A\ \Delta Y_A\ \Delta Z_A\ \Delta X_B\ \Delta Y_B\ \Delta Z_B\ \Delta X_M\ \Delta Y_M\ \Delta Z_M\ \Delta X_N\ \Delta Y_N\ \Delta Z_N \right)^T$, **A** and **B** are coefficient matrix, $\boldsymbol{V}$ and L are similar to Eq. 2.

Combine Eqs. 8, 14 and 15, we have

$$\begin{cases} \boldsymbol{V} = \boldsymbol{AT} + \boldsymbol{B}\hat{\boldsymbol{X}} - \boldsymbol{L} \\ \boldsymbol{C_1}\hat{\boldsymbol{X}}_{\boldsymbol{1}} + \boldsymbol{W_1} = \boldsymbol{0} \\ \boldsymbol{C_2}\hat{\boldsymbol{X}}_{\boldsymbol{2}} + \boldsymbol{W_2} = \boldsymbol{0} \end{cases} \qquad (16)$$

Further, we rewrite Eq. 16 by

$$\begin{cases} \mathbf{V} = \mathbf{D}\delta\mathbf{X} - \mathbf{L} \\ \mathbf{C}_x\delta\mathbf{X} + \mathbf{W}_x = \mathbf{0} \end{cases} \tag{17}$$

where $\mathbf{C_x} = \begin{pmatrix} \mathbf{C_1} & \mathbf{C_2} \end{pmatrix}^{\mathbf{T}}$, and $\boldsymbol{W_x} = \begin{pmatrix} \boldsymbol{W_1} & \boldsymbol{W_2} \end{pmatrix}^{\boldsymbol{T}}$, $\mathbf{D} = \begin{pmatrix} \mathbf{A} \mid & \mathbf{B} \end{pmatrix}$

$\boldsymbol{\delta X} = \begin{pmatrix} \Delta\varphi\ \Delta\omega\ \Delta\kappa\ \Delta X_S\ \Delta Y_S\ \Delta Z_S \Delta X_A\ \Delta Y_A\ \Delta Z_A \cdots \Delta X_N\ \Delta Y_N\ \Delta Z_N \end{pmatrix}^T$

With the least-squares establishment method (Lawson and Hanson, 1995), Eq. 17 can be written by

$$\boldsymbol{\Phi} = \mathbf{V}^{\mathbf{T}}\mathbf{V} + \mathbf{2K}_{\mathbf{s}}^{\mathbf{T}}(\mathbf{C}_x\delta\mathbf{X} + \mathbf{W_x})$$

The corresponding normal equation is:

$$\begin{cases} \mathbf{D}^{\mathbf{T}}\mathbf{D}\delta\mathbf{X} + \mathbf{C}_x{}^{\mathbf{T}}\mathbf{K_S} + \mathbf{D}^{\mathbf{T}}\mathbf{L} = \mathbf{0} \\ \mathbf{C}_x\delta\mathbf{X} + \mathbf{0}\mathbf{K_S} + \mathbf{W_X} = \mathbf{0} \end{cases} \tag{18}$$

where $\mathbf{K_S}$ is an introduced unknown matrix. If number of the total observation equations is m, $\mathbf{K_S}$ is a $m \times 1$ matrix, i.e., $\boldsymbol{K_S} = \begin{pmatrix} K_{S_1}, K_{S_2}, \cdots, K_{S_m} \end{pmatrix}^T$.

Let $N_{dd} = D^T D$, Eq. 18 is rewritten by

$$\begin{pmatrix} \mathbf{N_{dd}} & \mathbf{C}_x{}^{\mathbf{T}} \\ \mathbf{C}_x & \mathbf{0} \end{pmatrix}\begin{pmatrix} \boldsymbol{\delta}\mathbf{X} \\ \mathbf{K_s} \end{pmatrix} + \begin{pmatrix} \mathbf{D}^{\mathbf{T}}\mathbf{L} \\ \mathbf{W_x} \end{pmatrix} = \mathbf{0} \tag{19}$$

The solution of unknown parameters would be

$$\begin{cases} \boldsymbol{\delta}\mathbf{X} = -\left(\mathbf{Q_{11}}\mathbf{D}^{\mathbf{T}}\mathbf{L} + \mathbf{Q_{12}}\mathbf{W_X}\right) \\ \mathbf{K_S} = -\left(\mathbf{Q_{21}}\mathbf{D}^{\mathbf{T}}\mathbf{L} + \mathbf{Q_{22}}\mathbf{W_X}\right) \end{cases} \tag{20}$$

where

$$\begin{pmatrix} \mathbf{N_{dd}} & \mathbf{C}_x{}^{\mathbf{T}} \\ \mathbf{C_x} & \mathbf{0} \end{pmatrix}^{-1} = \begin{pmatrix} \mathbf{Q_{11}} & \mathbf{Q_{12}} \\ \mathbf{Q_{21}} & \mathbf{Q_{22}} \end{pmatrix} \tag{21}$$

Eq. 20 is a mathematical model to be used for orthorectification. As seen, this model combines the building relative controls and the traditional ground point control. Thus, higher accuracy of orthoimage should be achieved.

3. Successes and Accomplishments

Accuracy comparison of the generated high-resolution urban orthoimages was conducted through three methods. Method 1 only employs 8 ground control points; Method 2 used 232 GCPs; and Method 3 (our method) employs 76 relative control lines and 56 GCPs. The success of the developed approached can be demonstrated by the following two methods:

(1) *Visual check*: The wire lines derived from the DBM model, which is taken the "true" value, is superimposed onto the three orthorectified building roofs, respectively. Four orthorectified buildings with different heights and at different location are selected for visually checking their accuracy achievable (Figure 9). As seen, there are significant offsets between the building wire lines and the building edges in the orthoimage generated by Method 1. The average deviations for four buildings are approximately 15 pixels and 10 pixels along x and y directions. However, the average offsets from our method are only 1.0-1.5 pixels in both x and y directions. The results demonstrated that the accuracy of orthoimage generated by our method has been greatly increased.

(2) *Checkpoint check:* 89 checkpoints are employed to evaluate the absolute accuracy of the orthoimages orthorectified by three methods. The checkpoints are located in the corners of building and are considered as "true" value. The coordinates corresponding to the checkpoints in the three orthoimages are measured. The average deviation in both x and y direction are listed in Table 1. As seen from Table 3, the offsets from Method 1 and Method 2 have approximately 3-5 feet and 2-4 feet, respectively, while 0.5 -1.0 feet from our method. The results again demonstrated that our method can significantly improve the accuracy of the generated orthoimage.

Table 1 Accuracy comparison of orthorectified image

	Method 1 (feet)		Method 2 (feet)		Our method (feet)	
	ΔX	ΔY	ΔX	ΔY	ΔX	ΔY
Mean	3.621	4.874	2.918	3.977	0.78	1.125

As mentioned early, the relief displacements caused by high building occur along radial lines from the nadir point, which means that the relief displacements are zero for imaged objects at the

nadir point and increases with increased radial distances from the nadir. In order to exam how much the proposed method could improve the accuracy for the marginal and central objects, we measured the errors for the margin and central orthoimage, and found that the proposed method could improve the accuracy of orthoimage approximately 5-7 feet for those objects in the image margin, but approximate 0-1 pixel for those high-objects surrounding the nadir point (see Figure 9).

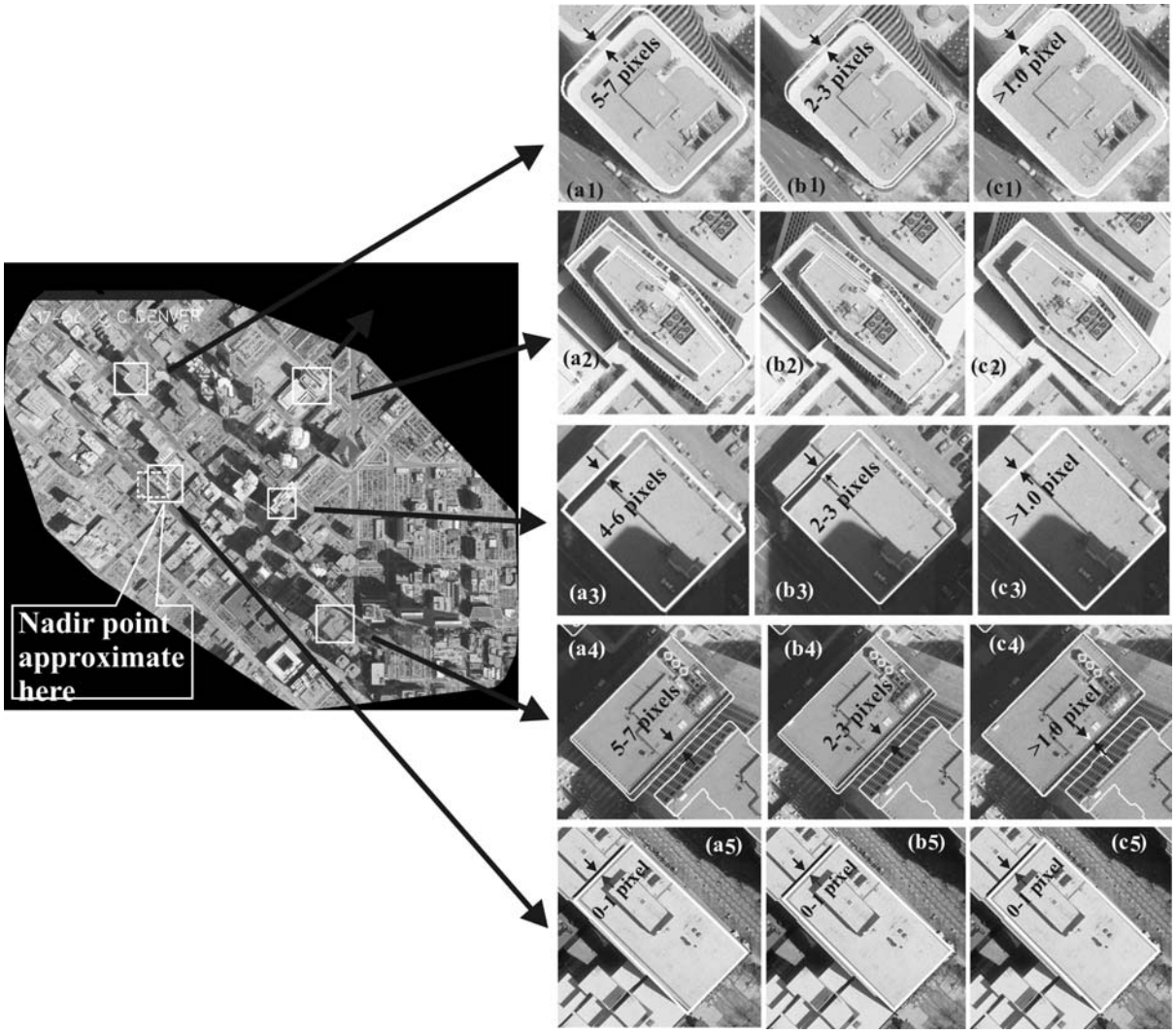

Figure 9 The comparison of building's orthorectification using three control condition: (a) 8 control points; (b) 232 ground control point; (c) 56 control points plus 76 control lines.

4. Completed Activities

This section would summarize the completed activities on the project, entitled "High-Resolution Urban True Orthoimagery Standard" funded by the NSDI Cooperative Agreements Program. In the beginning of the project, two tele-conferences were held on November 12, 2009 and December 8, 2009, respectively. The proposal of deploying the project activities was presented by the Principal investigator (PI) to the NSDI, and reviewed by two peer-reviewers specified by Federal Geographic Data Committee. With valuable inputs and comments from two reviewers, a draft of document pertain to the high-resolution urban true orthoimagery has been produced. This draft of the document describes process, accuracy, and quality control for urban high-resolution (e.g., 6-inch or one-foot) gray and color−infrared high-resolution digital orthoimagery in urban area. The descriptions in this document are different from those in the existing Standards such as (1) Geographic Information Framework Data Content Standard Part 2: Digital Orthoimagery (FGDC)*;* (2) Digital Orthophoto Standard formulated by the National Digital Orthophoto Program (NDOP); (3) Content Standards for Digital Orthophoto; (4) Digital Orthophoto Program formulated by USGS in 1998; (5) Standards for 1:12,000-scale orthophoto quarter-quadrangles, etc. This document is classified as a National Spatial Data Infrastructure by the Federal Geographic Data Committee (FGDC). In addition, a test using the high-resolution aerial imagery located in downtown Denver, Colorado, where the highest building is 125m, and many others are around 100m, with six original aerial images was conducted. The test experimental results exposed the problems of traditional orthoimage generation method such as ghost images, occlusion and building lean, shadow of the buildings, inaccuracy of DSM, incomplete refilling to occlusion, different geometric accuracy of adjacent orthoimages, etc. For this reason, the project presents a method which first established mathematical model of constrain conditions on the building edges, such as perpendicularity, and then merged these constrain conditions into the orthorectification model. A test field located in downtown of Denver, Colorado has been used to evaluate our methods. The experimental results demonstrated that the proposed method can improve the accuracy of 2-5 feet for those buildings of over 100 m high, and even 5-7 feet for those buildings over 100 m high in the margin of imagery (Zhou et al., 2008).

During the second half project year, the PI investigated the applications of high-resolution orthoimages in transportation pavement management at the Virginia Tech Transportation Institute (VTTI) at Blacksburg, VA and Environmental Research, Inc. (ERI) at Linden, VA. The investigation results indicated that they still used the traditional methods in the software, such as PCI, ERDAS/Imagine, etc to generate orthophotos from aerial image. In the meanwhile, the survey and evaluation form for high-resolution urban orthoimagery standard was conducted by mails and telephones. The survey contents included nine questionnaires in general and seven questionnaires in specification. The five forms were feedbacked from the mailed 20 forms. The survey by mails and telephones indicated that the current software, PCI, ERDAS/Imagine, etc., exposed some problems for urban high-resolution orthoimage generation, but the proposed Standards increase the procedures, cost and time of orthoimage generation, so that the most of private companies will be reluctant to admit such a Standard.

The outreach was also conducted at PI's photogrammetry course (CET411) in the 2010 Spring Semester at ODU. 20 students attended this class. Since the orthophoto generation (orthorectification) is one of the major chapters of photogrammetry course, lecture note, presentation, laboratory class data, and problems-solving exercises have been developed. The major content in the lecture coursework contains (1) orthophoto generation history, (2) traditional orthorectification methods including mathematical models (e.g., polynomial, differential rectification), input data (e.g., 2.5D DEM, original aerial images), gray resampling, ground coordinate, (3) true orthorectification including DTM-based orthophoto, DBM-based orthophoto, procedure of true orthophoto generation, (4) occlusion refilling and shadow removal, and (5) comparison between traditional orthophoto and true orthophoto in mountain area and urban area, for small-scale, medium, and large-scale aerial images. Upon finishing the lessons and exercises, students were requested to fill out survey forms to assess how much they benefited from the activities. The survey forms included questionnaires such as (1) Were the problems you studied interesting and exciting? (2) Did these activities help you develop a better understanding of orthorectification in urban area? (3) Did these activities help you develop a better understanding of urban orthorectificaiton issues? (4) Did these lessons increase your interest in pursuing an engineering career? (5) What did you like best/least about these lessons and exercises? (6) How could these lessons and exercises be improved? The surveyed results

demonstrated that the students benefited from the taught course on theory and method of urban high-resolution orthoimage generation.

5. Public Access and Deliverables

The deliverables of the project are majorly a final document describing the process, problem, challenges, accuracy, and quality control for urban high-resolution (e.g., 6-inch or one-foot) gray and color−infrared high-resolution digital orthoimagery in urban area. Especially, the problems and challenges encountered using the traditional orthoimage generation method have been highlighted, and the approach for resolving these challenges have been developed. A successful example is demonstrated. The experimental data for this test are deliverables for public users at no cost.

6. Activities Planned in the Future

Public accept to the new method of generating an orthoimage will still need many efforts. We plan to host a workshop in the future to bring together experts, professors, and users from U.S. universities, government agencies, industries, and organization, such as the Federal Geographic Data Committee (FGDC), the National Mapping Center (NMC), the National Geospatial Data Infrastructure (NGDI), the National States Geographic Information Council (NSGIC), and American Congress of Survey and Mapping (ACSM), American Society for Photogrammetry and Remote Sensing, (ASPRS), USGS regional Center: Mapping Applications Center-MAC (Reston, VA), Mid-Continent Mapping Center-MCMC (Rolla, MO); Rocky Mountain Mapping Center-RMMC (Denver, CO), FL Regional Office (Ocala, FL), KY Regional Office (Louisville, KY), MA Regional Office (Northborough, MA) and OH Regional Office (Columbus, OH), local government agencies, e.g., City of Norfolk, City of Virginia Beach, and private sections, such as ESRI Inc., and Leica Geo-System (formerly Erdas/Imagine) Inc. to discuss the new version of the *Standard*, in which some items for urban high-resolution orthophoto should be amended.

References

[1] FGDC (2008). Geographic Information Framework Data Content Standard Part 2: Digital Orthoimagery, May 2008, http://www.fgdc.gov/standards/projects/ FGDC-standards-projects/framework-data-standard/GI_FrameworkData Standard_Part2_DigitalOrthoimagery.pdf (last access on June 12, 2010).

[2] USGS, (1998). Digital Orthophoto Program, U.S. Department of the Interior, U.S. Geological Survey, http://mapping.usgs.goc/www/ndop/index.html

[3] USGS (1996). Digital Orthophoto Standards, *National Mapping Program−Technical Instructions*, **Part I, General**; **Part II, Specifications**. US Department of the Interior, U.S. Geological Survey, National Mapping Division. Dec. 1996. http://rmmcweb.cr.usgs.gov/public/nmpstds/doqstds.html.

[4] Federal Geographic Data Committee (1999). Content Standards for Digital Orthoimagery, February 1999 http://www.fgdc.gov/standards/projects/ FGDC −standards −projects/ orthoimagery/orth_299.pdf

[5] U.S. Geological Survey (1986). Standards for Digital Elevation Models: National Mapping Program Technical Instruction.

[6] U.S. Geological Survey (1991). Standards for 1:12,000−scale Orthophoto Quarter−Quadrangles: National Mapping Program Technical Instructions, 18 p.

[7] U.S. Geological Survey (1992). Standards for 1:24,000−scale Orthophoto Quadrangles: National Mapping Program Technical Instructions, 20 p.

[8] Federal Geographic Data Committee (1995). Development of a National Digital Geospatial Data Framework, April, 1995, http://www.fgdc.gov/framework /framdev.html.

[9] Federal Geographic Data Committee (1997). Fact sheet: National Digital Geospatial Data Framework: A Status Report, Federal Geographic Data Committee, July 1997, 37p. http://www.fgdc.gov /framework/framdev.html, July, 1997.

[10] Zhou, G., W. Xie, and P. Cheng (2008). Orthoimage creation of high buildings, *IEEE Tran. On Geoscience and Remote Sensing,* vol. 46, no. 12, Dec. 2008, pp. 4132 – 4141.

[11] Zhou, G., W. Chen, and J. Kelmelis (2005). A comprehensive study on urban aerial image orthorectification for national mapping program, *IEEE Trans. on Geosciene and Remote Sensing*, vol. 43, no. 9, pp. 2138-2147.

[12] Zhou, G., W. Schickler (2004a). True orthoimage generation in extremely tall building urban areas, *International Journal of Remote Sensing*, vol. 25, no. 22, pp. 5161-5178.

[13] Zhou, G., K. Jezek (2004b). Satellite orbital parameters-assisted orthorectification for satellite imagery over 60° N latitude, *Photogrammetric Engineering and Remote Sensing*, vol. 70, no. 9, 2004, pp. 1021-1029.

[14] Zhou, G. K. Jezek, (2002), Orthorectifying 1960's disclassified intelligence satellite photography of Greenland, *IEEE Tran. on Geoscience and Remote Sensing,* vol. 40, no. 6, 2002, pp. 1247-1259.

Feedback on Cooperative Agreements Program

(1) What are the CAP Program strengths and weaknesses?

Answer: The CAP Program strengths are its focus on the national geospatial data. The weaknesses are (1) when the applicant's idea is not consistent with the CAP Program experits', no chance to discuss or exchange this idea although the CAP experts are erroneous.

(2) Where does it make a difference?
Answer: The format on the submittal report.

(3) Was the assistance you received sufficient or effective?
Answer: Fair.

(4) What would you recommend that the FGDC do differently?
Answer: no recommendation.

(5) Are there factors that are missing or additional needs that should be considered?
Answer: too less financial support, but much workload.

(6) Are there program management concerns that need to be addressed, such as the time frame?
Answer: Too many the repeated email communications with senseless request.

(7) If you were to do this again, what would you do differently?
Answer: Do not know.